Numerical Analysis of An 80,000 Nm^3/h Fly Ash Entrained-Flow Gasifier At Various Burner Inclination Angles

Neng Fang

Institute of Engineering Thermophysics, Chinese Academy of Sciences, Beijing, 100190, P.R. China; School of Energy Science and Engineering, Harbin Institute of Technology, 92, West Dazhi Street, Harbin 150001, P.R. China

Lingyan Zeng (zenglingyanhit@126.com)

School of Mechanical Engineering, Shanghai Dianji University, Shanghai, 201306, P.R. China; School of Energy Science and Engineering, Harbin Institute of Technology, 92, West Dazhi Street, Harbin 150001, P.R. China https://orcid.org/0000-0002-4583-002X

Yue Lu

School of Energy Science and Engineering, Harbin Institute of Technology, 92, West Dazhi Street, Harbin 150001, P.R. China

Zhengqi Li

School of Energy Science and Engineering, Harbin Institute of Technology, 92, West Dazhi Street, Harbin 150001, P.R. China

Zhichao Chen

School of Energy Science and Engineering, Harbin Institute of Technology, 92, West Dazhi Street, Harbin 150001, P.R. China

Research Article

Keywords: Entrained-flow gasification, Raw syngas, Fly ash, Burner inclination angle

Posted Date: August 23rd, 2021

DOI: https://doi.org/10.21203/rs.3.rs-662402/v1

Version of Record: A version of this preprint was published at Environmental Science and Pollution Research on December 2nd, 2021. See the published version at https://doi.org/10.1007/s11356-021-17770-2.

Abstract

The raw syngas effluent from a fluidized bed gasifier typically contains a large amount of fly ash having a high concentration of carbon, which is undesirable. The present work examined the newly developed entrained-flow gasification technology intended to gasify raw syngas. Simulation of gas-solid flow and reaction behavior in an industrial-scale entrained-flow gasifier applying this new technology was first performed to obtain a better understanding of the particle flow and gasification characteristics. In addition, the devolatilization and heterogeneous reactions of fly ash particles were characterized by thermogravimetric analysis and user-defined function. The predictions from the simulation showed good agreement with the results of in situ experimental measurements. The combustion reaction for raw syngas occurred in the burner jet zone. As the hot gaseous products diffused, gasification reactions dominated the other zones. When burner inclination angle was 0°, 8.5°, and 25.5°, the temperature at the bottom outlet of the gasifier was lower than the ash fusion temperature with the value of 1360 °C. Solid slag formed and blocked the outlet. By comparison, this gasifier with the burner inclination angle of 17° could discharge the liquid slag and function as a continuous operation. In this way, the carbon conversion in fly ash reached the maximum value of 89.5%.

Introduction

Coal gasification which converts elements C and H from coal into effective syngas ($CO + H_2$) is the key technology for clean and efficient utilization of coal and production of coal-based chemicals (Chang et al., 2016). Industrial coal gasifiers are usually categorized into the fixed bed gasifier, the fluidized bed gasifier, and the entrained-flow gasifier (Wu et al., 2010; Dogru and Erdem, 2019; Pan et al., 2016; Ayola, Yurdakos and Gurgen, 2019; Li et al., 2018; Tamošiūnas et al., 2019; Zeng et al., 2014). Fluidized bed gasification develops rapidly in China's coal chemical industry and occupies a large market share due to its advantages of high heat and mass transfer efficiency, mature process, high annual operation rate, and low production cost (Matsuoka et al., 2013). Unfortunately, the operating temperature of the fluidized bed gasifier is low at about 900–1000 ℃, so the char particles formed by coal devolatilization only undergo partial combustion and gasification reactions, and eventually form fly ash with higher carbon content. A large amount of fly ash was contained in the generated raw syngas, which reduces the quality of syngas and even affects the stable operation of the gasifier system (Chen, Namioka and Yoshikawa, 2011; Xu et al., 2010).

To mitigate the above problems, post-treatment systems for the removal of fly ash are typically installed at the gasifier outlet. These systems successively include cyclones, bag dust collectors, and various wet removal processes. In the case of a cyclone separator, only the larger particles (> 5 μm) are separated and returned to the gasifier chamber through the return conduit, while the remaining fly ash is carried into a bag dust collector by the flow of the raw syngas. Much of the fly ash is then captured by the filter cake on top of the bag filter material, such that the relatively small fly ash particles (0.1-5 μm) are separated. The remaining material with particle sizes less than 0.1 μm has to be removed using a wet process, such as a spray tower, wash tower, or Venturi tube scrubber (Yoshida, Ono and Fukui, 2005; Wang et al., 2013),

employing a liquid as the dust collector to capture particles from the gas stream. This type of post-treatment system suffers from several challenges. First, the high rate of water consumption required makes such processes unsuitable for use in regions where water is scarce. Second, the sewage generated by the wet removal has to be treated, which significantly increases costs. Finally, these physical removal processes cannot reduce the carbon content in the fly ash.

The fly ash contained in the raw syngas from a fluidized bed gasifier tends to have a high carbon content (20–40%) (Kelebopile, Sun and Liao, 2011; Ouyang et al., 2018). The fly ash particles are internally porous, have loose structures, and are readily crushed. In addition, the pores in these particles can absorb significant amounts of water and high-temperature sintering loss. These characteristics together tend to restrict the potential utilization of fly ash as a raw material. As such, the dry ash separated from the bag dust collector cannot be used to make cement or concrete admixtures, or to produce foamed glass or ceramics. In addition, the wet ash filtered from the sewage is mud-like and can contain numerous pollutants, such as heavy metals and small amounts of tar and phenol. This material is also inconvenient to transport and cannot be used directly. Therefore, fly ash recovered from post-treatment systems is often simply disposed of via landfill (Hurt et al., 1998), even though this is not a sustainable option as it uses valuable land and can lead to environmental degradation (Ahmaruzzaman, 2010). Discarding fly ash also represents a monetary loss because this material contains a significant quantity of unburned carbon and thus could serve as fuel in a fluidized bed combustor. Ouyang et al. (Ouyang et al., 2018) investigated the combustion characteristics and NO_x emissions associated with the coal gasification of fly ash in a 0.4 MW preheated combustion test rig, and found a maximum fly ash combustion efficiency of 98.6% with NO_x emissions of 155 mg/Nm^3. Some commercial processes (Blissett and Rowson, 2012) also use fly ash as a secondary fuel, which removes most of the unburned carbon in fluidized bed combustors. However, there have been few reports focused on the gasification of fly ash using an entrained-flow gasifier.

A novel technology for the purification of raw syngas has been developed in which fly ash is treated in an entrained-flow gasifier after coming directly came from a fluidized bed. This process is referred to as fly ash entrained-flow gasification, and the first 80,000 Nm^3/h fly ash entrained-flow gasifier was constructed in Liaoning, China in 2015 (Fang et al., 2020). As this unit can be considered to be dilute-phase entrained-flow reactors, it does not directly gasify pulverized coal, but have the same advantages as coal entrained-flow gasifiers. In addition, because the fine ash is rapidly heated in this system to generate molten particles, the unburned carbon is almost completely exhausted, while the remaining ash forms a liquid slag that is discharged from the gasifier. In this manner, a fly ash entrained-flow gasifier effectively converts the small particles into raw syngas. Consequently, this kind of gasifier can replace the wet removal equipment in a typical fly ash post-treatment system while removing the generation of sewage and lowering equipment costs. This process can also reduce the carbon content in the fly ash to less than 3% while recycling the carbon and energy from the fly ash.

In view of the extensive application of numerical simulation to visually provide detailed information on the complex process of reactions in gasifiers (Wu et al., 2010; Hurt et al., 1998; Myöhänen, Palonen and

Hyppänen, 2018; Li et al., 2020; Fang et al., 2019; Chen, Hung and Chen, 2012), a comprehensive three-dimensional numerical simulation was developed to get a full understanding of the particle flow and gasification characteristics in industrial-scale fly ash entrained-flow gasifier. The operating conditions can affect the performance of a gasifier. The structural parameters also have a significant impact on the operation performance, although these effects have only rarely been researched. Adjusting the burner inclination angle helps to optimize the design of the gasifier. Therefore, the present work assessed the effects of different burner inclination angles (0°, 8.5°, 17°, and 25.5°) on the flow and reaction behaviors in a gasifier.

80,000 Nm3/h Fly Ash Entrained-flow Gasifier

The schematic drawing of the 80,000 Nm^3/h fly ash entrained-flow gasifier is illustrated in Fig. 1. The coordinate origin is located at the bottom of the gasification chamber. *z* is the distance to the gasifier exit along the height direction, and the settings of *x* and *y* are presented. The wall of the gasification chamber is constituted by firebricks made by China Luoyang Institute of Refractories Research Ltd. On the wall at the same height above the bottom of 3.13m, six burners are evenly arranged along the peripheral direction. From the top view, all burners deviate β from the gasifier center. And in the vertical plane, all burners incline the horizontal direction by α (referred to as burner inclination angle). Five measuring points (port1, port2, port3, port4, and port5), in the same perpendicular direction, are distributed in the middle of two adjacent burners. From the center to outward, two parallel channels are concentrically arranged in the burner, i.e., the central channel and the outer channel respectively convey the gasifying agent and raw gas. In the raw syngas, the volume percentage of CO, H_2, CO_2, and H_2O is 19.4%, 24.30%, 13.0%, and 40.1%, respectively. The amount of N_2 and CH_4 is very small, about 1.12% and 1.98%. According to the GB/T219 and GB/T1574, the characteristics of fly ash in the raw syngas are listed in Table 1.

Table 1
Specifications of the fly ash in the raw syngas.

Items	Data
Proximate Analysis (wt %, dry)	
Volatile matter	8.3
Fix carbon	36.5
Ash	55.2
High heating value ($MJ{\cdot}kg^{-1}$)	15.3
Ultimate analysis (wt %, dry ash free)	
Carbon	91.2
Hydrogen	1.2
Oxygen	4.7
Nitrogen	1.2
Sulfur	1.7
Deformation temperature (℃)	1260
Softening temperature (℃)	1290
Fusion temperature (℃)	1360

The inlet raw syngas came from an Ende circulating fluidized bed gasifier (Liu et al., 2019). Liquid slag is discharged from the bottom outlet of the gasifier, while the gaseous products escape from the top outlet into the waste heat boiler. The fly ash entrained-flow gasifier pressure (gauge pressure) is 11.5 kPa, and the operating parameters are shown in Table 2.

Table 2
Operating parameters of the fly ash entrained-flow gasifier.

Channel	Components	Mass flow rate ($kg\ h^{-1}$)	Velocity ($m\ s^{-1}$)	Temperature(°C)
Central channel	O_2	10989	27.5	107
	H_2O (g)	594	27.5	107
Outer channel	Raw syngas	65787	80.1	832
	Fly ash	6721		832

Model Description And Simulation Method

3.1. General description

Measuring the particle flow and gasification characteristics in a real gasifier directly (Niu et al., 2008a; Yan et al., 2009; Niu et al., 2008b; Zhong et al., 2009) is difficult because of the enormous risk of leakage and explosion of combustible gas. As a more cost-effective mean, three-dimensional numerical simulation was conducted using the Fluent software (version 6.3). Gas turbulence was taken into consideration by the realizable k-ε model (Shih, Lion and Shabbir, 1995). The Lagrangian stochastic tracking model was applied to analyze the particle motion, while calculations of gas/particle two-phase coupling employed a discrete phase model (Gosman and Loannides, 1981). Radiation was described using the DO model (Lu and Wang, 2013). The non-premixed combustion model with the secondary stream (Fang et al., 2019; Bi et al., 2015) was used to model the turbulence-chemical interactions. Fly ash and raw syngas were respectively represented as empirical fuel steam and secondary steam.

3.2. Particle reactions model

Because the mass fraction of volatile in fly ash was less than 10%, the simple one-step model (Badzioch and Hawksley, 1970) was applied to describe the devolatilization process. The reaction rate R_v is calculated as follows:

$$R_v = m_c A \exp(E / RT)$$

where m_c and T are the mass of volatile in particles (kg) and particle temperature (K), respectively. The pre-exponential factor A, and activation energy E obtained from the thermogravimetric analysis are 2.72×10^7 $s^{-1}$and 140 kJ mol^{-1}, respectively.

The fixed carbon of fly ash mainly reacts with H_2O and CO_2, while it also reacts with O_2 in the oxygen-rich area. In order to accurately describe the heterogeneous reactions of fly ash, the kinetic parameters were introduced to the non-premixed combustion model using the user-defined function (UDF). Related calculations can be found in the literature (Fang et al., 2019). The values of the pre-exponential factor and activation energy are given in Table 3.

Table 3
Kinetic parameters for heterogeneous reactions.

	$C+O_2$ [a]	$C+H_2O$ [b]	$C+CO_2$
A (s^{-1})	1.12×10^7	6.42×10^5	1.76×10^6
E (kJ mol^{-1})	141	211	325
Note: a refers to (Jing et al., 2014), b refers to (Jing, Wang and Fang, 2013).			

The kinetic parameters in the fly ash devolatilization process were measured by using the thermogravimetric-differential scanning calorimetry mode of a STA449C thermal analyzer. Before the experiment, a separate blank run was performed for baseline correction. After the vacuum operation,

about 5 mg sample was loaded into an alumina crucible. The sample was warmed from room temperature to 110 ° C, and then was dried and dehydrated by constant temperature for 10 minutes. The sample was heated under an N_2 atmosphere (60 mL/min) up to 1200°C with heating rates of 35°C/min. Kinetics characteristics of fly ash and CO_2 were also investigated under the CO_2 atmosphere. Finally, kinetic parameters were obtained by distributed activation energy models (Blázquez, Zamora and Calero, 2017). The thermogravimetric analysis had an error of less than 5%. Detail methods of tests and data calculations were described in the literature (Wang et al., 2018).

3.3. Grid meshing and algorithm

ANSYS ICEM software was used in this work. The structured hexahedral mesh was used in global geometry, and it was refined near the burners. Owing to the symmetry flow field in the gasification chamber, 1/6 of its grid (see Fig. 2) was employed as a computational domain. The boundary condition for the symmetric plans was “periodic”. Grid-dependent tests were conducted with three grid systems of approximately 610,000, 888,000, and 1,205,000 cells and revealed the grid independence. The grid of 888,000 was adopted to balance the speed and accuracy of calculations.

The pressure-velocity coupling was described by SIMPLE algorithm. The “PRESTO” scheme was used to discretize the pressure and the “second-order upwind” scheme was chosen for the other terms. These discretized equations were solved by the pressure-based implicit method.

Results And Discussion

4.1 Model verification

The purified syngas at the top outlet of the fly ash gasifier was cooled via a spray of water to avoid overheating the waste heat boiler. The exit syngas in the simulation and experiment was sampled after the fly ash gasifier and waste heat boiler respectively, so their results cannot be directly compared. However, the results of in situ temperature measurements at a distance of less than 50 mm from the gasifier wall (with a burner inclination angle of 17°) are shown in Fig. 3 and are compared with those acquired from simulations. The range of measurement error is the maximum deviation obtained from multiple measurement statistics. The platinum-rhodium thermocouples covered with a corundum ceramic shield were used to measure the temperature. Meanwhile, the measurement range of the thermocouple was 0 ~ 1550°C, and the measurement error for the gasifier constructed of firebricks was less than that for gasifier formed by cooling screens with the range of 1.4%-8.0% (De, 2019). Here the thermocouples were inserted through the holes opened on the firebricks (the measurement ports were presented in Fig. 1). The predictions from the numerical simulations are all consistent with the experimental values, with discrepancies of less than 100°C. This agreement indicates that the models used in the present research are suitable for predicting the performance of the fly ash entrained-flow gasifier.

4.2 Flow field and velocity distribution

The velocity vector on the *x-z* plane is seen in Fig. 4**(a)**. The flow field in fly ash entrained-flow gasifier at a burner inclination angle of 17° can be divided into five regions: the jet zone (JZ), swirling mixture zone (SZ), recirculation zone (RZ), upper swirling flow zone (USZ) and lower swirling flow zone (LSZ). Both the gasifying agent and raw syngas flow into the gasification chamber and form the JZ, after which the airflows from all six JZs are rotated and mixed in the SZ. These two zones can be distinguished along the *z*-direction of the velocity vector and there is a surrounding recirculation zone between the wall and the JZ. The boundary between the JZ and RZ is defined herein as the edge at which the velocity is 5% of the initial velocity of the raw syngas. The hot gaseous products entrained by recirculation can lead to high-temperature corrosion of the burner and nearby wall, and therefore thermal protection should be provided for these regions. The upper and lower swirling flow zones are divided by the SZ and RZ, and extend to the top and bottom outlet of the gasification chamber, respectively. Because the six burners deviate from the horizontal plane at specific downward angles, the majority of each airflow descends downward from the SZ, impinges on the sloping wall at the bottom of the gasification chamber, and then flows upward. There are also some airflows that directly diffuse upward.

The radial distribution of axial velocity on different elevations is presented in Fig. 4**(b)**. *r* denotes the radial distance from the gasifier axis. The plane that passes through the center of the burner exit and is parallel to the *x-y* plane is defined as the burner plane, and the vertical height of the burner plane is 3130 mm. Here, *R* is the diameter of a specific cross-section and, as r/R increases (i.e., moving radially outward from the gasifier center), the axial velocity on the burner plane first decreases on going to the trough and then increases to a maximum at the radial position $r/R = 0.4$. This represents the boundary between the JZ and SZ. This effect occurs because the convergence of airflows from two adjacent burners strengthens both flows in the axial direction and leads to a peak velocity. In the JZ ($r/R > 0.4$), the axial velocity first decreases to zero then continues to decrease on going to the trough, at which point it increases slightly. At the cross-sections at $z = 2.5$ and 1.5 m, the radial positions at which the axial velocity is zero near the gasifier axis ($r/R = 0.73$ and 0.87, respectively) are the boundaries between the RZ and the JZ. At the cross-section at $z = 6$ m, the initial value of the axial velocity has a small negative value, indicating that there is a weak recirculation zone in the center of the section. As r/R increases, the axial velocity increases to a peak and then slowly decreases.

4.3 Temperature and species distribution

The temperature distribution on the *x-z* plane (a) and burner plane (b) under the burner inclination angle of 17° is shown in Fig. 5. The combustion reaction of the raw syngas occurs in the JZ, in which the gasification agent is surrounded by the raw syngas and the two flows are injected in parallel from the burner. The initial temperature of the syngas is 832°C, which exceeds its ignition point, so a flame extends from the outer surface of the gasification agent to the center, generating a V-shaped structure in which the maximum temperature is about 2220°C. The flame inclines downward, such that the region underneath the flame is heated much more rapidly than in other areas. In addition, as the hot gaseous products diffuse, the temperatures in the SZ, RZ, and LSZ all exceed 1650°C. Oxygen is consumed rapidly in the JZ, so a high-temperature, strongly reductive environment is formed in the other zones, which

favors the gasification of the fly ash entrained by the raw syngas. It is important to note that the sloping wall at bottom of the gasification chamber must be able to withstand the corrosive airflow and temperatures up to 1830°C as well as the scouring effect of the fly ash. Thus, the firebricks in this area are made of a material with high chromium content. The temperature at the bottom outlet of the gasification chamber is approximately 1527°C, so liquid slag is discharged from this outlet. Because of the cooling effect provided by a portion of the raw syngas that diffuses directly upward from the JZ, the temperature in the USZ gradually decreases to 1330°C along the *z*-direction.

Figure 6 and **Figure 7** respectively present the mole fraction contours of CO and H_2 on the *x*-*z* plane (a) and burner plane (b) under the burner inclination angle of 17°. As a result of the relatively high oxygen concentration in the center of the JZ, both CO and H_2 are rapidly consumed in this region. In addition, the H_2 concentration in the vicinity of the burner outer channel is much higher than that in the USZ, while the CO concentrations in these two zones are similar. During the combustion reaction between the raw syngas and oxygen, H_2 is also consumed, and the cold gas efficiency values before and after the fly ash entrained-flow gasifier are 60.5% and 59.9%, respectively.

4.4 Particle distribution and residence time of fly ash

The particle concentration contours on the *x*-*z* plane (a) and burner plane (b) under the burner inclination angle of 17° are given in Fig. 8. The fly ash particles are primarily distributed at the bottom outlet and the straight wall near the top outlet of the gasifier. The temperature of the latter region is nearly 1330°C (see Fig. 5) and is slightly lower than the flow temperature of the fly ash. A small amount of solid slag may be formed under these conditions, but would not be expected to block the top outlet because the majority of the ash is transformed to liquid slag and discharged from the bottom outlet. After the prolonged operation of the gasifier, any blockages tend to accumulate on the straight wall near the top outlet and subsequently slide downwards under their weight.

The trajectory distribution of fly ash particles in the gasification chamber under the burner inclination angle of 17° is plotted in Fig. 9. The residence times of the fly ash particles in units of seconds are indicated by colors. Most particles undergo a helical motion as they move through the SZ, LSZ, and USZ successively, so that their trajectories are close to the wall surface. As a result, the pathlength that the particles travel over is quite long and their average residence time is more than 6 s, which tends to increase the conversion rate of carbon in the fly ash. Some particles escape directly from the SZ and passed through the USZ with a smaller radius of rotation, resulting in a reduction of the residence time by half.

4.5 Influence of different burner inclination angles

The temperature distribution in the lower gasification chamber at various burner inclination angles is shown in Fig. 10. Increasing the burner inclination angle from 0° to 25.5° transfers the high-temperature zone (>1700 ℃) from the center of the gasifier to the inclined wall below the burner. In practical usage, burner inclinations of 17° and 25.5° may result in damage to the inclined wall. It is also evident that the

offset of the V-shaped flame in all four cases is extremely small because the pressure difference between the burner exit and the top outlet of the gasifier is sufficiently large such that the gasifying agent and the raw syngas quickly shift upward after leaving the burner. At burner inclination angles of 0°, 8.5°, and 25.5°, the temperatures at the bottom outlet of the gasifier are lower than the ash fusion temperatures (see Table 1), such that solid slag will form and block the outlet. This effect is attributed to the movement of the high-temperature zone away from the bottom outlet. In contrast, a burner inclination of 17° produces a temperature greater than 1500 ℃, so the fly ash entrained-flow gasifier can discharge the liquid slag and function as a continuous operation.

Modifying the oxygen-to-carbon ratio is commonly used to tune the temperature in the gasifier (Matteo et al., 2013; Xu et al., 2016; Kong et al., 2014). Changing the stoichiometric ratio between the gasification agent and the coal (including biomass, fly ash, and other carbonaceous combustibles) varies the intensity of the combustion reaction and thus affects the temperature values throughout the gasifier. However, this parameter has limited influence on the distribution of the combustion area and flow field. In the present work, the burner inclination angle was examined as an adjustable structural parameter, and simulated variations in this angle were found to dramatically affect the distribution of the high-temperature zone. This effect could be beneficial in terms of addressing the problems of solid slag blocking the outlet and burning of the gasifier wall.

The axial velocity fields in the lower gasification chamber at various burner inclination angles are given in Fig. 11. The burner inclination angle has only a minimal effect on the distributions of the JZ and LSZ. As the burner inclination angle increases from 0° to 17°, the maximum velocity in the SZ gradually increases while the size of the SZ decreases. In contrast, when the burner inclination angle increases to 25.5°, the maximum velocity in the SZ decreases and that zone becomes slightly larger. The recirculation zone above the JZ expands while that below the JZ shrinks when increasing the burner inclination angle from 0° to 25.5°.

Figure 12 presents the effects of burner inclination angle on effective syngas concentration and carbon conversion of fly ash at the gasifier exit. As the angle increases from 0° to 17°, the mole fraction of the effective syngas and the rate of carbon conversion in the fly ash at the gasifier outlet both increase. However, an angle of 25.5° reduces both of these variables. These two parameters characterize the gasification efficiency and show maximum values of 0.363 and 89.5%, respectively, when the burner inclination angle is 17°. Based on safety considerations and optimizing the gasification efficiency in fly ash entrained-flow gasifier, the optimal burner inclination angle is evidently 17°. This angle would allow the continuous stable operation of the gasifier while reducing the effective gas consumption and improving the conversion of carbon in the fly ash.

Conclusions

The present work reported on a numerical investigation into particle flow and gasification characteristics within an 80,000 Nm^3/h fly ash entrained-flow gasifier. Effects of the burner inclination angles (0°, 8.5°,

17°, and 25.5°) on the gasification efficiency were determined. The non-premixed combustion model with the secondary stream was adopted, and the heterogeneous reactions of fly ash were described by a user-defined function. The conclusions are as follows:

(1) The flow field in the gasifier can be divided into five regions: jet zone (JZ), swirling mixture zone (SZ), recirculation zone (RZ), upper swirling flow zone (USZ) and lower swirling flow zone (LSZ). The combustion reaction of raw syngas occurred in the JZ. As the diffusion of the hot gaseous products, gasification reactions were dominant in the other zones.

(2) Most particles underwent a helical motion through the SZ, LSZ, and USZ successively, so their trajectories were close to the wall surface and their average residence time was more than 6 s. Some particles escaped directly from the SZ and passed through the USZ with a much shorter residence time.

(3) At burner inclination angles of 0°, 8.5° and 25.5°, the temperatures at the bottom outlet of the gasifier were lower than the ash fusion temperatures (1360 ℃), such that solid slag would form and block the outlet. In contrast, the burner inclination of 17° produced a temperature greater than 1500 ℃, so the gasifier was able to discharge the liquid slag and functioned as a continuous operation.

(4) The mole fraction of effective syngas ($CO + H_2$) and carbon conversion rate of fly ash at the gasifier outlet which characterized the gasification efficiency showed maximum values of 0.363 and 89.5% respectively at the burner inclination angle of 17°. This optimal setting was recommended based on safety considerations and optimizing the gasification efficiency.

Declarations

Authors' information

Corresponding author: *Tel: +86 451 8641 3231, Fax: +86 451 8641 3209. E-mail: zenglingyanhit@126.com (Lingyan Zeng).

Authors Contributions

Neng Fang: Conceptualization, Methodology, Validation, Writing - Original Draft. Lingyan Zeng: Writing-Reviewing and Editing, Supervision. Yue Lu: Investigation, Data curation. Zhengqi Li: Resources. Zhichao Chen: Project administration.

Funding

This work was supported by the National Key R&D Program of China (2017YFB0602001).

Availability of data and materials

The datasets used and/or analysed during the current study are available from the corresponding author on reasonable request.

Competing interests

The authors declare that they have no competing interests.

Ethics approval and consent to participate

Not applicable.

Consent for publication

Not applicable.

References

1. Ahmaruzzaman M (2010) A review on the utilization of fly ash. Prog Energy Combust Sci 36:327–362. https://www.sciencedirect.com/science/article/abs/pii/S0360128509000604
2. Ayola A, Yurdakos OT, Gurgen A (2019) Investigation of municipal sludge gasification potential: gasification characteristics of dried sludge in a pilot-scale downdraft fixed bed gasifier. Int J Hydrogen Energy 44:17397–17410. https://www.sciencedirect.com/science/article/abs/pii/S0360319919300576
3. Badzioch S, Hawksley PGW (1970) Kinetics of thermal decomposition of pulverized coal particles. Ind Eng Chem Process Des Dev 9:521–530. https://www.sciencedirect.com/science/article/abs/pii/S0082078481801257
4. Bi DP, Guan QL, Xuan WW, Zhang JS (2015) Numerical simulation of GSP gasifier under different swirl angles. Fuel 155:155–163. https://www.sciencedirect.com/science/article/abs/pii/S0016236115003828
5. Blázquez G, Zamora MC, Calero M (2017) Kinetic modelling of torrefaction of olive tree pruning. Apply Thermal Engineering 113:1410–1418. https://www.sciencedirect.com/science/article/abs/pii/S1359431116334974
6. Blissett RS, Rowson NA (2012) A review of the multi-component utilisation of coal fly ash. Fuel 97:1–23. https://www.sciencedirect.com/science/article/abs/pii/S0016236112002335
7. Chang SY, Zhuo JK, Meng S, Qin SY, Yao Q (2016) Clean coal technologies in China: current status and future perspectives. Engineering 2:447–459. https://www.sciencedirect.com/science/article/pii/S2095809917300814
8. Chen CJ, Hung CI, Chen WF (2012) Numerical investigation on performance of coal gasification under various injection patterns in an entrained flow gasifier. Appl Energy 100:218–228. https://www.sciencedirect.com/science/article/abs/pii/S0306261912003613
9. Chen HF, Namioka T, Yoshikawa K (2011) Characteristics of tar, NO_x precursors and their absorption performance with different scrubbing solvents during the pyrolysis of sewage sludge. Appl Energy 88:5032–5041. https://www.sciencedirect.com/science/article/abs/pii/S0306261911004521

10. De DS (1982) Measurement of flame temperature with a multi-element thermocouple. J Inst Energy 54:113–118. https://core.ac.uk/display/199260761
11. Dogru M, Erdem A (2019) Process intensification and miniaturization in gasification technology: downdraft gasification of sugarcane bagasse. Energy Fuels 33:340–347. https://pubs.acs.org/doi/10.1021/acs.energyfuels.8b03460
12. Fang N, Li ZQ, Xie C, Liu SX, Zeng LY, Chen ZC, Zhang B (2020) The application of fly ash gasification for purifying the raw syngas in an industrial-scale entrained flow gasifier. Energy 195:117069. https://www.sciencedirect.com/science/article/abs/pii/S0360544220301766
13. Fang N, Zeng LY, Zhang B, Li ZQ, Wang HP, Liu XY (2019) Numerical simulation of flow and gasification characteristics with different swirl vane angles in a 2000t/d GSP gasifier. Appl Therm Eng 153:791–799. https://www.sciencedirect.com/science/article/abs/pii/S135943111835261X
14. Gosman AD, Loannides E (1981) Aspects of computer simulation of liquid-fueled combustors. AIAA 19th Aerospace Science Meeting 81:323–333. https://arc.aiaa.org/doi/10.2514/3.62687
15. Hurt R, Sun J, Lunden M (1998) A kinetic model of carbon burnout in pulverized coal combustion. Combust Flame 113:181–197. https://www.sciencedirect.com/science/article/abs/pii/S001021809700240X
16. Jing XL, Wang ZQ, Fang YT (2013) Steam regasification properties and kinetics of coal char fines derive d from fluidize d bed gasifier (in Chinese). Journal of Fuel Chemistry Technology 41:400–406
17. Jing XL, Wang ZQ, Zhang Q, Fang YT (2014) Combustion property and kinetics of fine chars derive d from fluidize d bed gasifier (in Chinese). Journal of Fuel Chemistry Technology 42:13–19
18. Kelebopile L, Sun R, Liao J (2011) Fly ash and coal char reactivity from thermo-gravimetric (TGA) experiments. Fuel Process Technology 92:1178–1186. https://www.sciencedirect.com/science/article/pii/S0378382011000257
19. Kong XD, Zhong WM, Du WL, Qian F (2014) Compartment modeling of coal gasification in an entrained flow gasifier: A study on the influence of operating conditions. Energy Convers Manag 82:202–211. https://www.sciencedirect.com/science/article/abs/pii/S0196890414001009
20. Li XG, Zeng LY, Liu HY, Song MH, Li WJ, Han H, Zhang SF, Chen ZC, Li ZQ (2020) Numerical simulation investigations into the influence of the mass ratio of pulverized-coal in fuel-rich flow to that in fuel-lean flow on the combustion and NO*x* generation characteristics of a 600-MW down-fired boiler. Environ Sci Pollut Res 27:16900–16915. https://pubmed.ncbi.nlm.nih.gov/32144700
21. Li ZQ, Fang N, Gao LS, Zeng LY, Chen ZC, Wang HP, Dong XB (2018) PDA research on the air/particle flow characteristics in a 2000 t/d GSP pulverized coal gasifier at different swirl vane angles. Fuel Process Technol 173:216–228. https://www.sciencedirect.com/science/article/pii/S0378382017317629
22. Liu XY, Chen ZC, Gao LS, Zhang J, Wang HP, Fang N, Li ZQ, Zeng LY, Song MH (2019) Reducing the unburned combustible in the fly ash from a 45,000 Nm^3/h Ende Pulverized-Coal Gasifier by applying steam-solid ejector. Appl Therm Eng 149:34–40. https://www.sciencedirect.com/science/article/abs/pii/S1359431118352049

23. Lu XJ, Wang T (2013) Investigation of radiation models in entrained-flow coal gasification simulation. Int J Heat Mass Transf 67:377–392. https://www.sciencedirect.com/science/article/abs/pii/S0017931013006716
24. Matsuoka K, Hosokai S, Kato Y, Kuramoto K, Suzuki Y, Norinaga K, Hayashi JI (2013) Promoting gas production by controlling the interaction of volatiles with char during coal gasification in a circulating fluidized bed gasification reactor. Fuel Process Technology 116:308–316. https://www.sciencedirect.com/science/article/pii/S0378382013002579
25. Matteo G, Giampaolo M, Ennio M, Ahmed FG (2013) Reduced order modeling of the Shell-Prenflo entrained flow gasifier. Fuel 104:822–837. https://www.sciencedirect.com/science/article/abs/pii/S0016236112005479
26. Myöhänen K, Palonen J, Hyppänen T (2018) Modelling of indirect steam gasification in circulating fluidized bed reactors. Fuel Process Technol 181:10–19. https://www.sciencedirect.com/science/article/pii/S0378382017310792
27. Niu MR, Yan ZY, Guo QH, Liang QF, Yu GS, Wang FC, Yu ZH (2008a) Experimental measurement of gas concentration distribution in an impinging entrained-flow gasifier. Fuel processing technology 89:1060–1068. https://www.sciencedirect.com/science/article/pii/S0378382008000854
28. Niu MR, Zhou WX, Yan ZY, Guo QH, Liang QF, Wang FC, Yu ZH (2008b) Multifractal detrended fluctuation analysis of combustion flames in four-burner impinging entrained-flow gasifier. Chem Eng J 143:230–235. https://www.sciencedirect.com/science/article/abs/pii/S138589470800212X
29. Ouyang ZQ, Liu W, Zhu JG, Liu JZ, Man CB (2018) Experimental research on combustion characteristics of coal gasification fly ash in a combustion chamber with a self-preheating burner. Fuel 215:378–385. https://www.sciencedirect.com/science/article/abs/pii/S0016236117314497
30. Pan CC, Liang QF, Guo XL, Dai ZH, Liu HF, Gong X (2016) Characteristics of different sized slag particles from entrained-flow coal gasification. Energy Fuels 30: 1487–1495. https://www.semanticscholar.org/paper/Characteristics-of-Different-Sized-Slag-Particles-Pan-Liang/7484e4cf05b6a46cdb6fd7445585548b9a55d82d
31. Shih TH, Lion WW, Shabbir A (1995) A new k-ε eddy viscosity model for high Reynolds number turbulent flows. Comp Fluids 24:227–238. https://www.sciencedirect.com/science/article/abs/pii/004579309400032T
32. Tamošiūnas A, Gimžauskaitė D, Uscila R, Aikas M (2019) Thermal arc plasma gasification of waste glycerol to syngas. Appl Energy 251:113306. https://www.sciencedirect.com/science/article/pii/S0306261919309687
33. Wang HP, Chen ZC, Zhang XY, Li ZQ, Fang N, Liu XY (2018) Thermal decomposition mechanisms of coal and coal chars under CO_2 atmosphere using a distributed activation energy model. Thermochim Acta 662:41–46. https://www.sciencedirect.com/science/article/abs/pii/S0040603118300406
34. Wang QL, Chen XL, Gong X (2013) The particle removing characteristics in a fixed valve tray column. Ind Eng Chem Res 52:3441–3452. https://pubs.acs.org/doi/10.1021/ie3027422

35. Wu YX, Zhang JS, Smith PJ, Zhang H, Reid C, Lv JF, Yue GX (2010) Three-Dimensional Simulation for an Entrained Flow Coal Slurry Gasifier. Energy Fuels 24:1156–1163. https://pubs.acs.org/doi/full/10.1021/ef901085b
36. Xu CB, Donald J, Byambajav E, Ohtsuka Y (2010) Recent advances in catalysts for hot-gas removal of tar and NH_3 from biomass. Fuel 89:1784–1795. https://www.sciencedirect.com/science/article/abs/pii/S0016236110000633
37. Xu JL, Zhao H, Dai ZH, Liu HF, Wang FC (2016) Numerical simulation of opposed multi-burner gasifier under different coal loading ratio. Fuel 174:97–106. https://www.sciencedirect.com/science/article/abs/pii/S0016236116001009
38. Yan ZY, Liang QF, Guo QH, Yu GS, Yu ZH (2009) Experimental investigations on temperature distributions of flame sections in a bench-scale opposed multi-burner gasifier. Appl Energy 86:1359–1364. https://www.sciencedirect.com/science/article/abs/pii/S0306261908002419
39. Yoshida H, Ono K, Fukui K (2005) The effect of a new method of fluid flow control on submicron particle classification in gas-cyclones. Powder Technol 149:139–147. https://www.sciencedirect.com/science/article/abs/pii/S0032591004004176
40. Zeng X, Wang F, Li HL, Wang Y, Dong L, Yu J, Xu GW (2014) Pilot verification of a low-tar two-stage coal gasification process with a fluidized bed pyrolyzer and fixed bed gasifier. Appl Energy 115:9–16. https://www.sciencedirect.com/science/article/abs/pii/S0032591004004176
41. Zhong C, Shuai Y, Liang QF, Wang FC, Yu ZH (2009) Distribution of HCN, NH3, NO and N2 in an entrained flow gasifier. Chem Eng J 148:312–318. https://www.sciencedirect.com/science/article/abs/pii/S1385894708005664

Figures

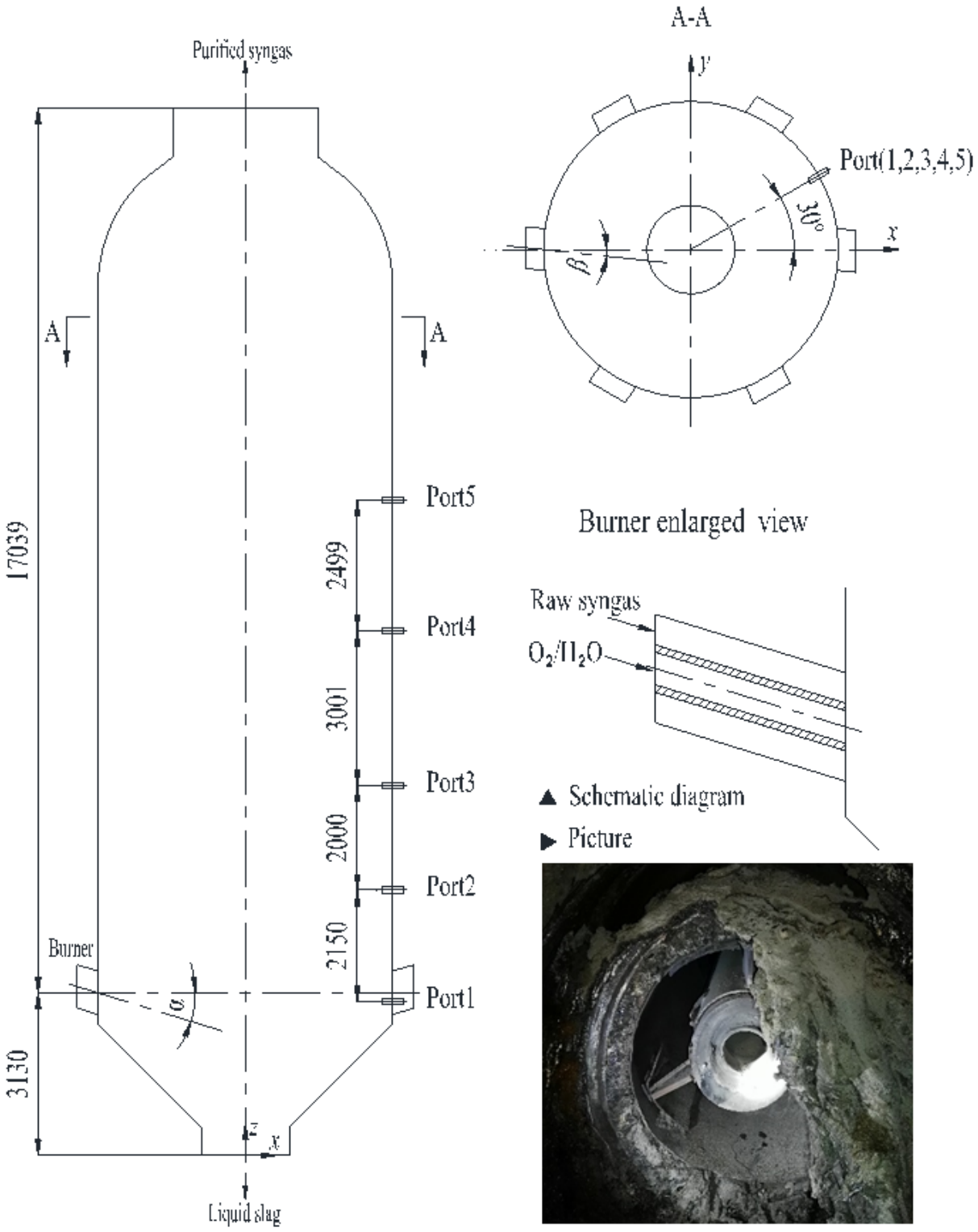

Figure 1

Schematic drawing of the 80,000 Nm3/h fly ash entrained-flow gasifier (unit: mm).

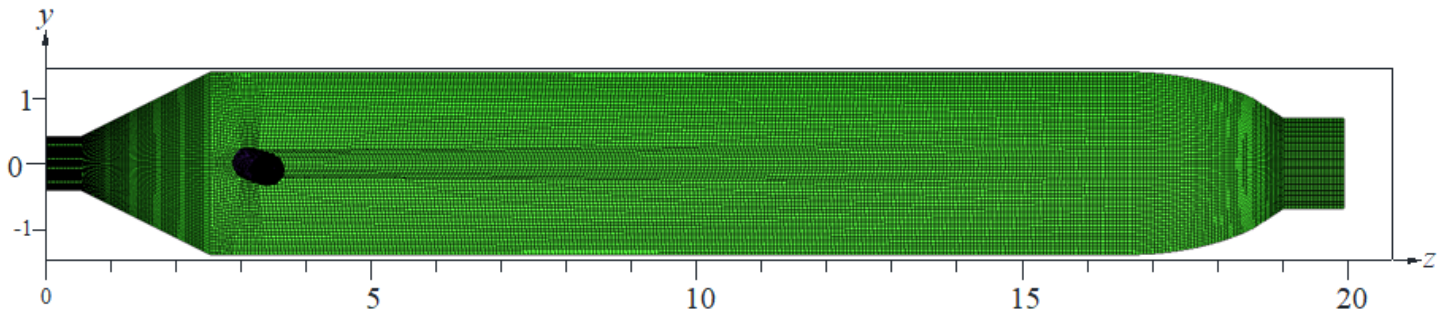

Figure 2

Grid divisions (unit: m).

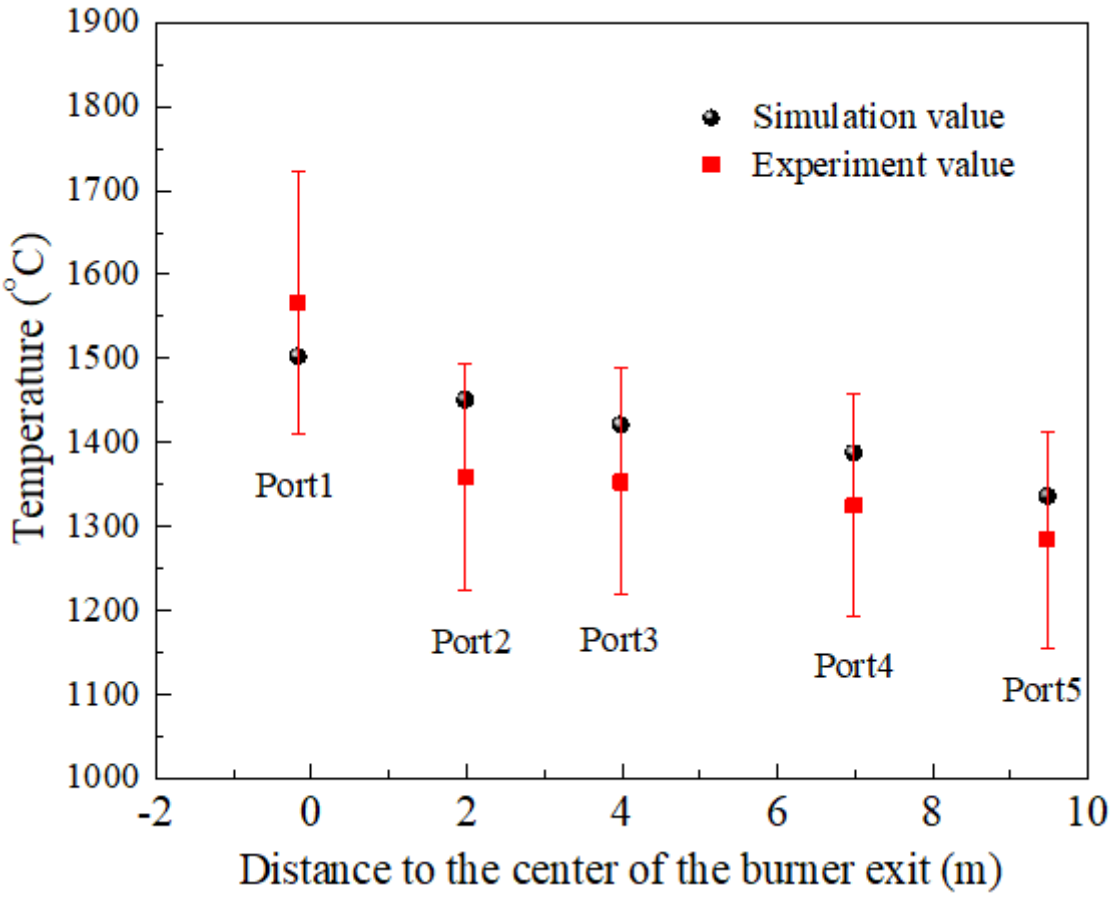

Figure 3

Distribution of temperatures near the wall of the gasification chamber.

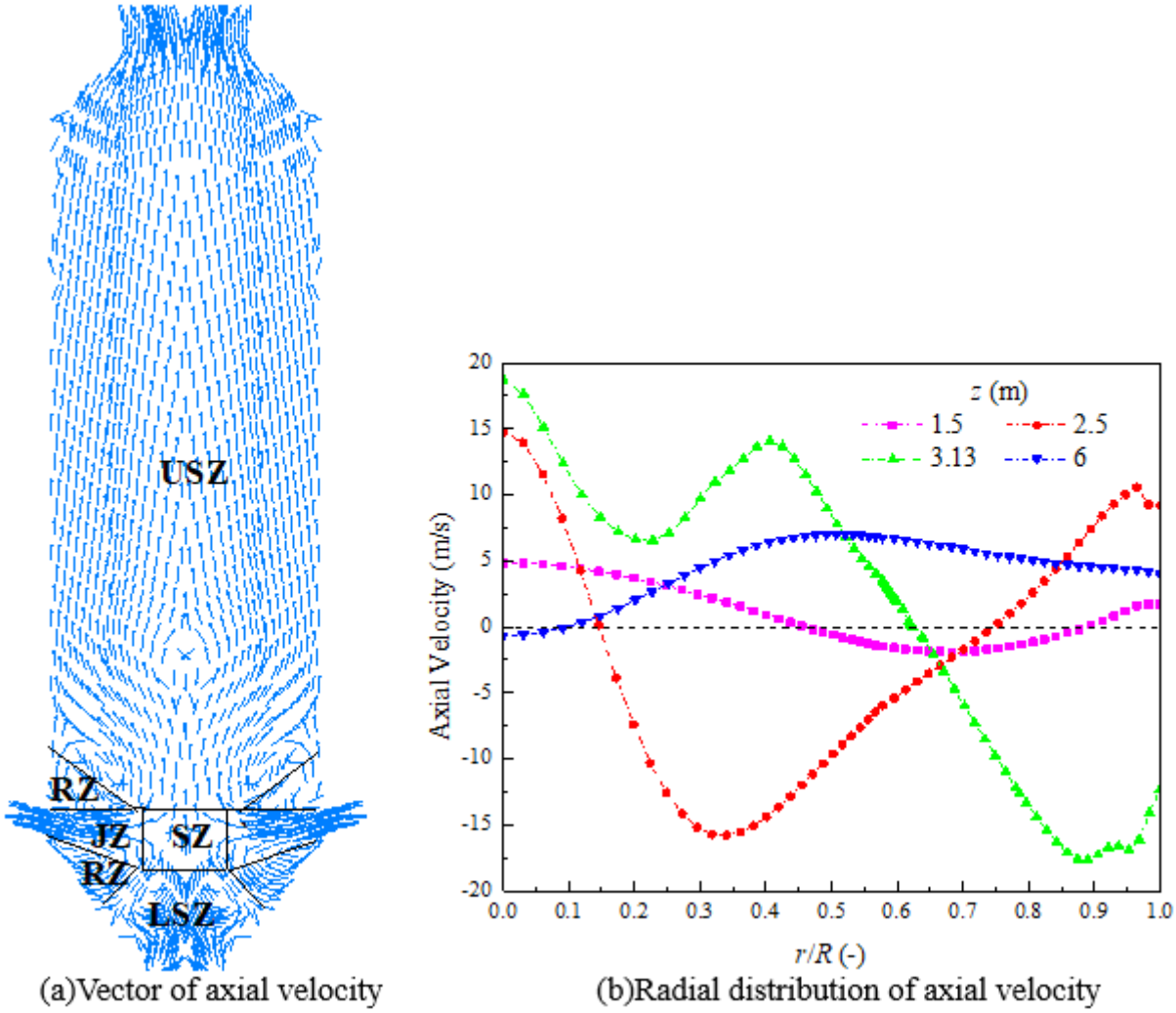

(a)Vector of axial velocity

(b)Radial distribution of axial velocity

Figure 4

Display of the axial velocity.

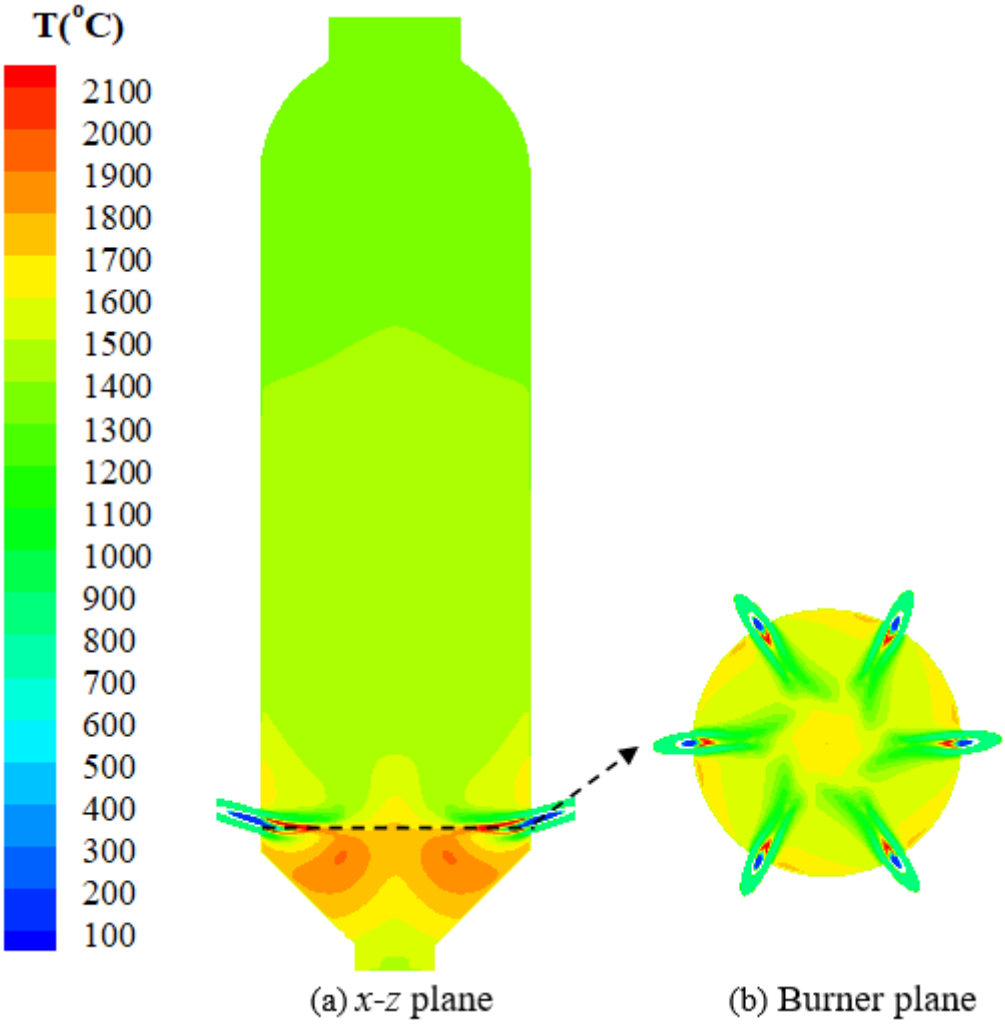

Figure 5

Temperature contour.

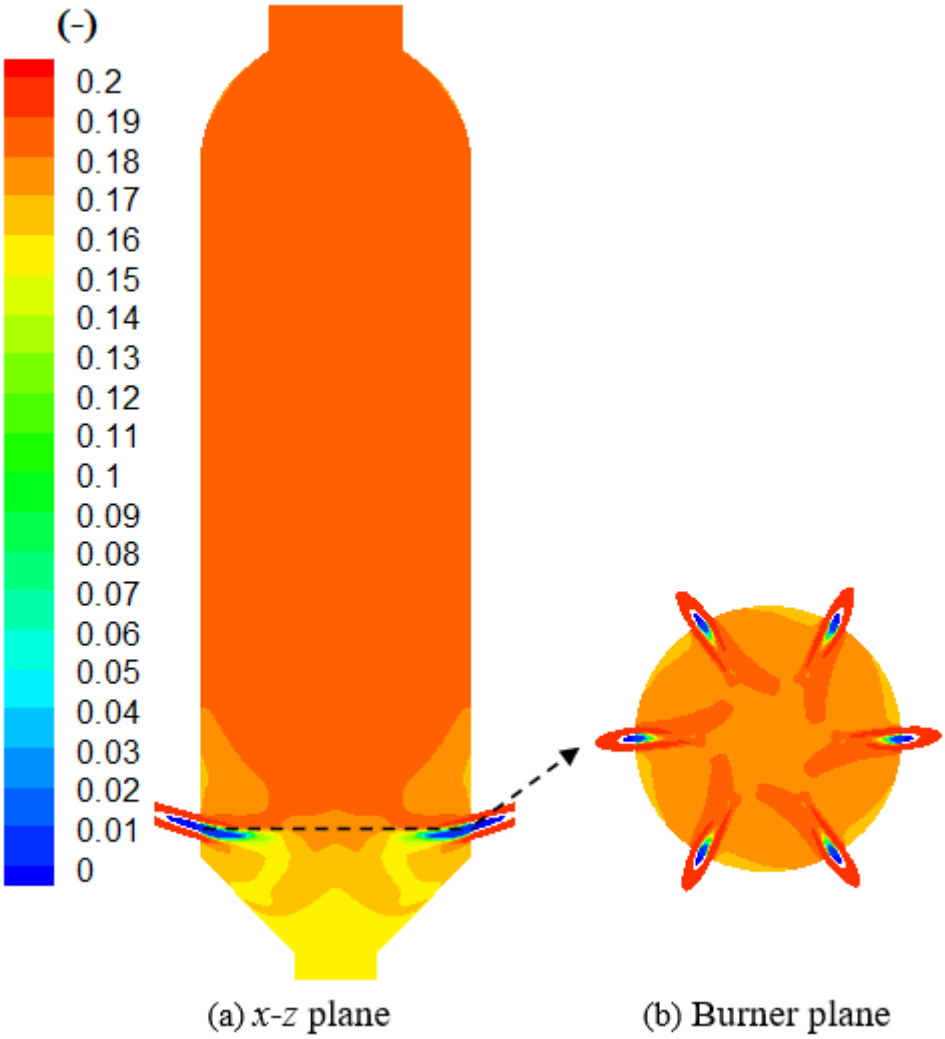

Figure 6

Mole fraction of CO.

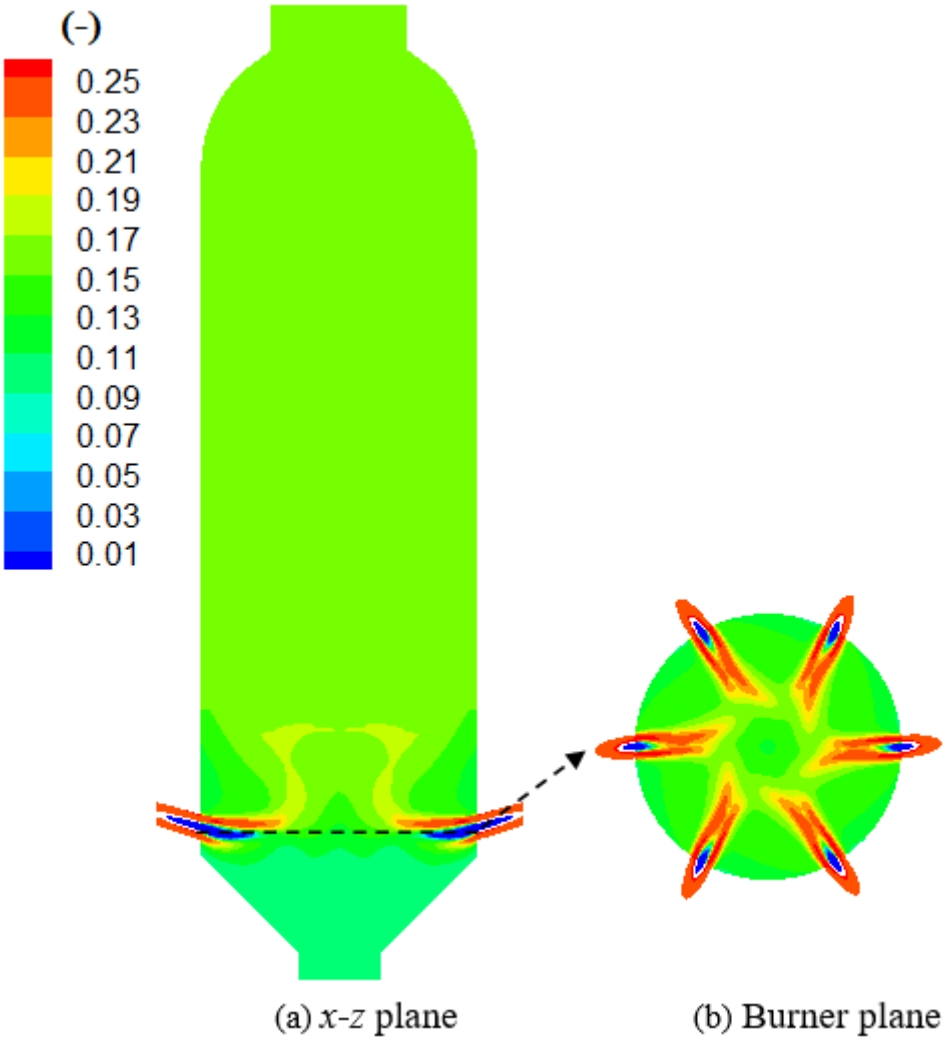

Figure 7

Mole fraction of H2.

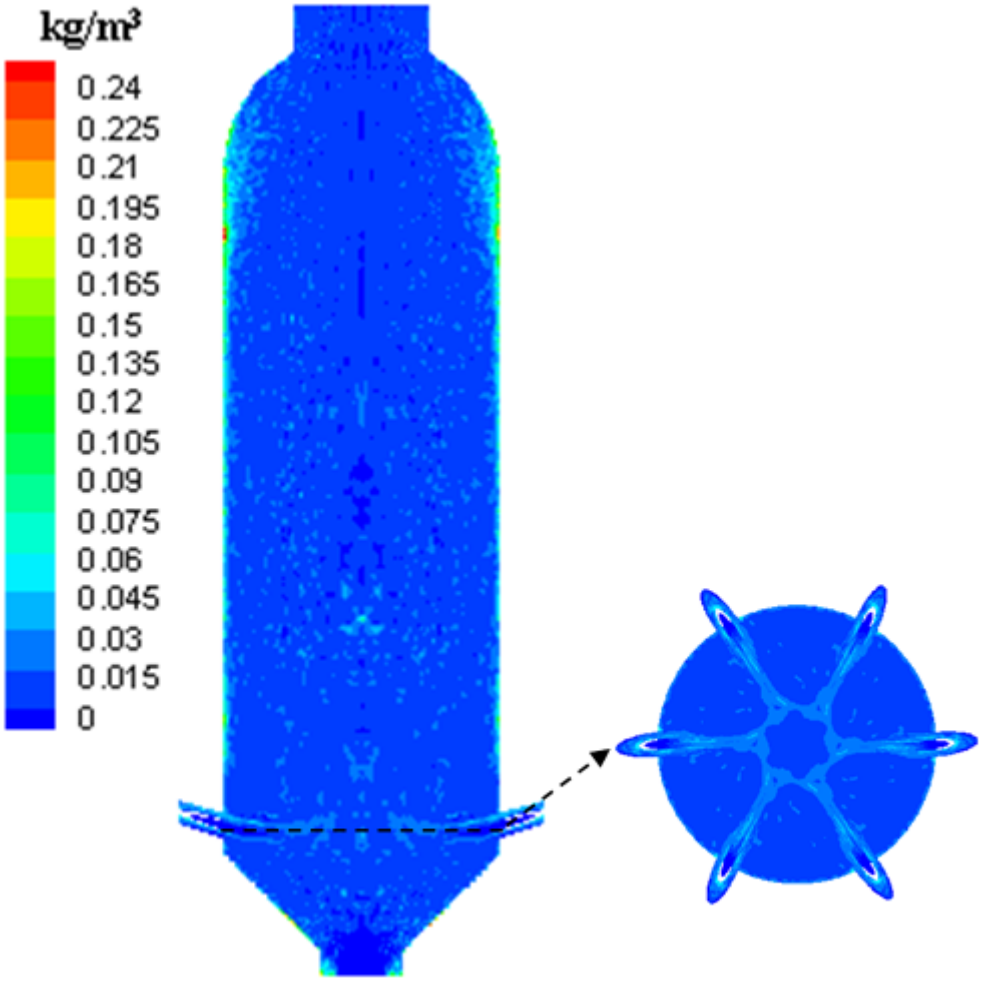

Figure 8

Concentration distribution of particles.

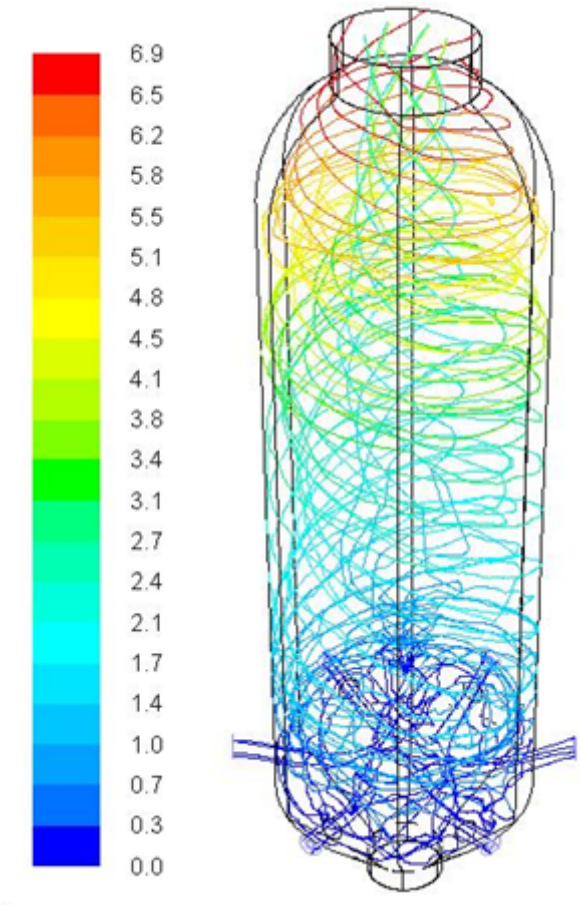

Figure 9

Trajectory distribution of fly ash particles in the gasification chamber.

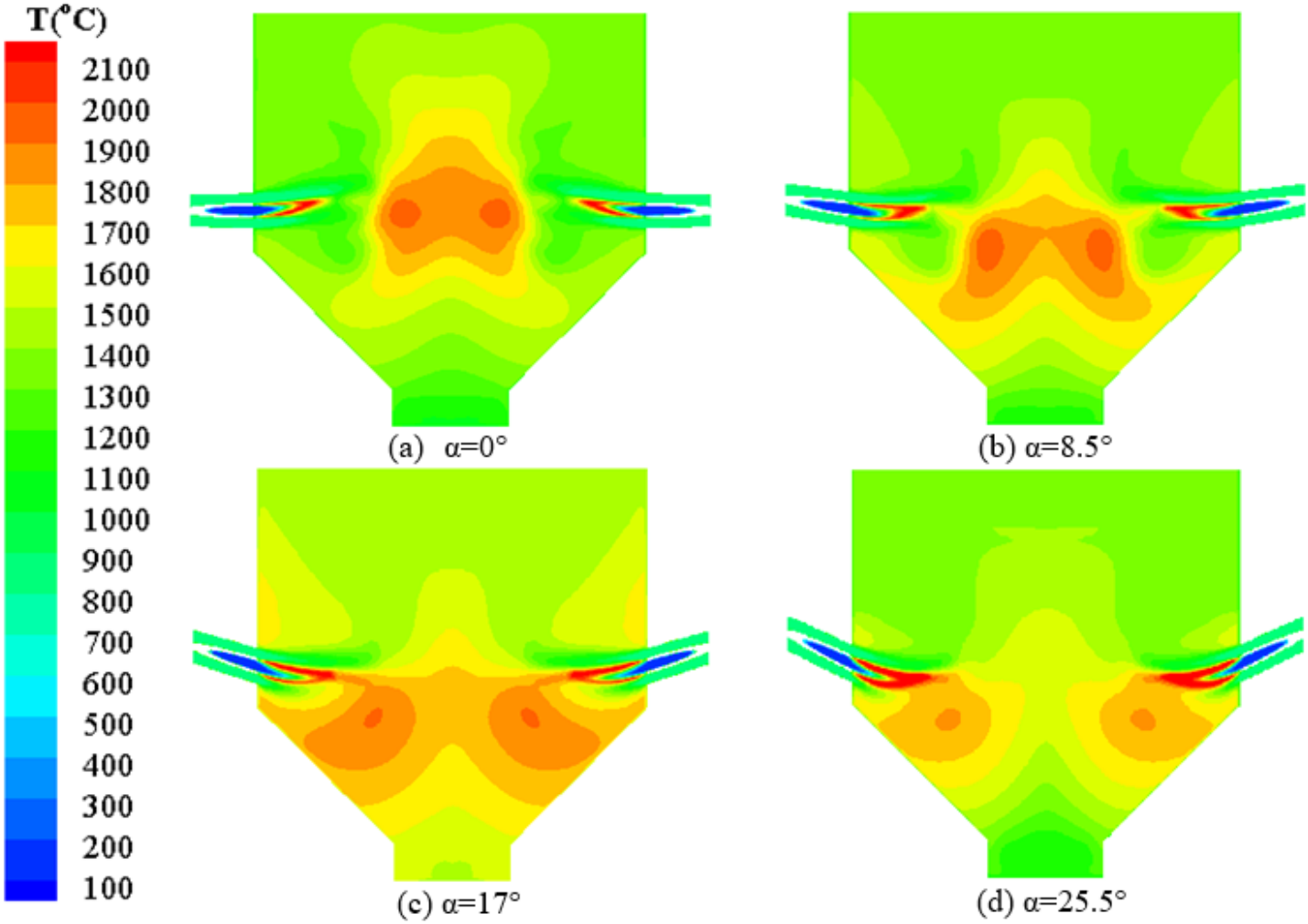

Figure 10

Temperature contours at various burner inclination angles.

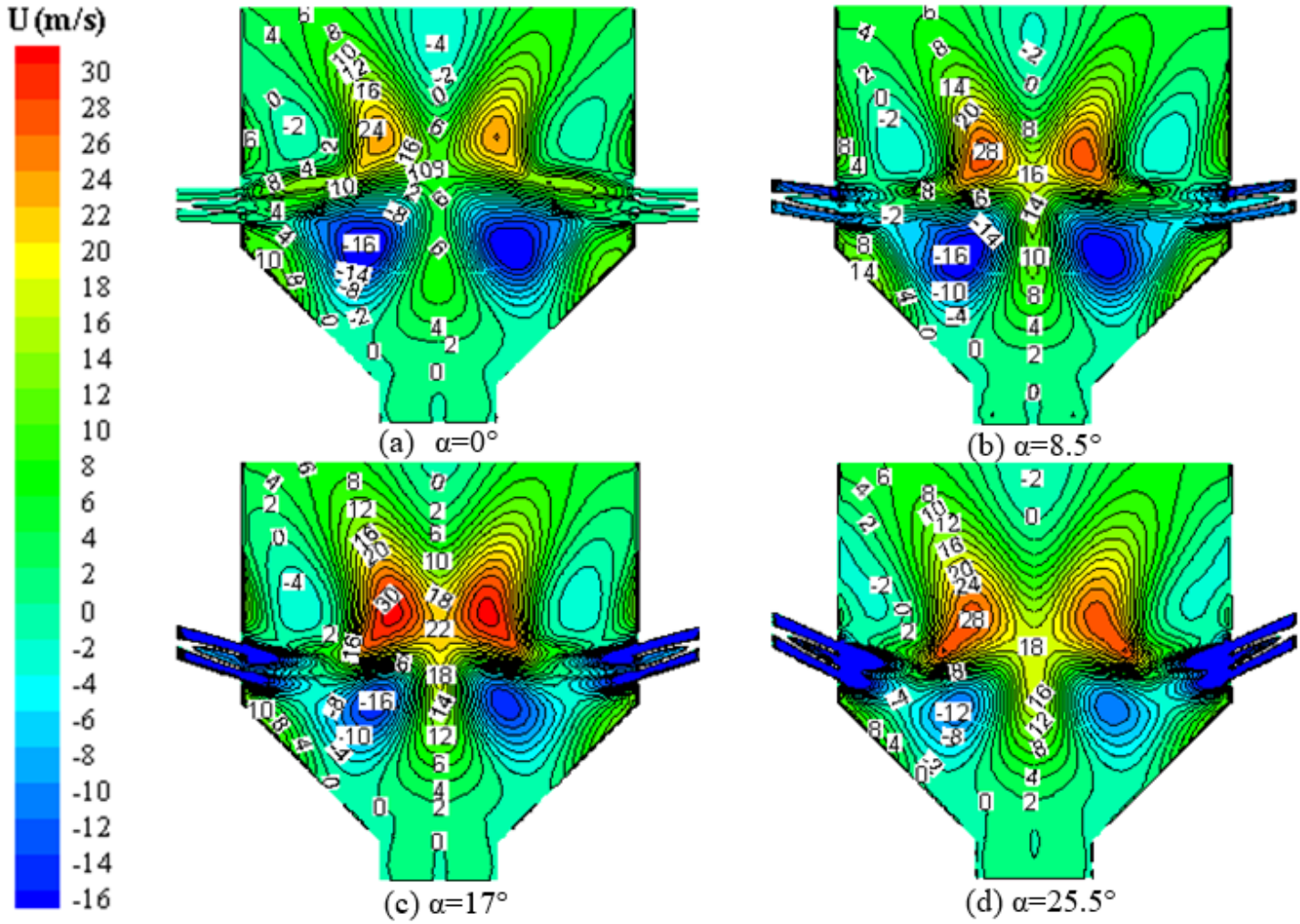

Figure 11

Axial velocity distributions at various burner inclination angles.

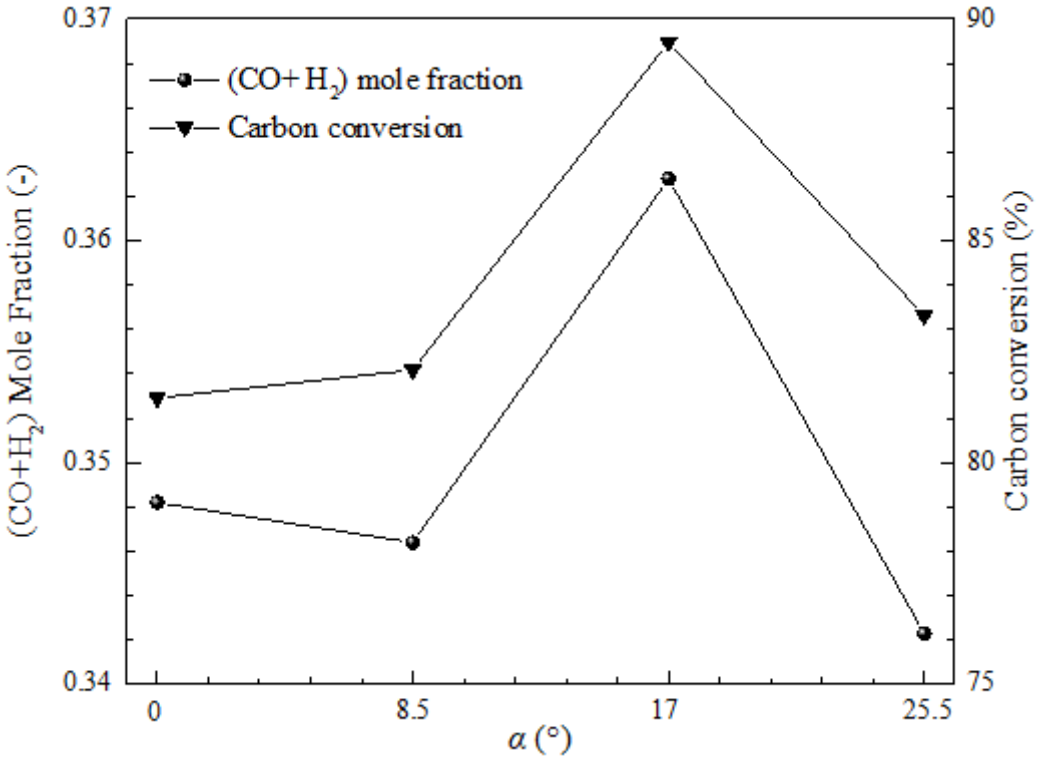

Figure 12

Effective syngas concentration and carbon conversion of fly ash.